Solar Energy Materials & Solar Cells 141 (2015) 232–239

Contents lists available at ScienceDirect

Solar Energy Materials & Solar Cells

journal homepage: www.elsevier.com/locate/solmat

Solution-processed interlayer of n-type small molecules for organic photovoltaic devices: Enhancement of the fill factor due to ordered orientation

Ho Jun Song [a], Eui Jin Lee [b], Doo Hun Kim [b], Doo Kyung Moon [b,1], Sangkug Lee [a,*,1]

[a] Cungcheong Regional Division IT Convergence Material R&D Group, Korea Institute of Industrial Technology, 89 Yangdaegiro-gil, Ipjang-myeon, Seobuk-gu, Cheonan-si, Chungcheongnam-do 331-822, Republic of Korea
[b] Department of Materials Chemistry and Engineering, Konkuk University, 1 Hwayang-dong, Gwangjin-gu, Seoul 143-701, Republic of Korea

ARTICLE INFO

Article history:
Received 11 February 2015
Received in revised form
23 April 2015
Accepted 28 April 2015
Available online 17 June 2015

Keywords:
Small molecule
Interlayer
OPVs
Orientation

ABSTRACT

Novel alcohol/water-soluble small molecules were obtained using various p- and n-type backbones. The synthesized molecules were dissolved in organic solvents and highly polar solvents. The DPPA film exhibited strong shoulder peak at approximately 633 nm compared with the solution, which was due to the ordered orientation of DPPA. According to XRD measurements, a prominent diffraction peak at 20.1° was observed in the in-plane diffraction pattern of DPPA, which indicates an out-of-plane peak (010) due to the molecular packing by π–π stacking. A photovoltaic device containing DPPA exhibited an open-circuit voltage of 0.75 V, a current density of 15.1 mA/cm^2, a fill factor of 69.0% and a power conversion efficiency of 7.9%. The photovoltaic device containing the DPPA derivative exhibited an improved power conversion efficiency compared with those containing BPA and QA (6.6% and 7.6%, respectively) due to the ordered orientation and packing of DPPA.

1. Introduction

Conjugated polymers have been widely used in organic light emitting diodes (OLEDs) [1–4], organic photovoltaic cells (OPVs) [5–11] and organic thin film transistors (OTFTs) [12,13] for several decades. On several occasions, OPVs have drawn considerable attention for these applications due to the universal technology tendency toward economic potential and continuative growth coupled with efforts to preserve the environment. However, the poor power conversion efficiency (PCE) of these materials has been the greatest barrier in organic photovoltaic development [6].

To improve these poor PCEs, various efforts continue to be applied to control the materials of the active layer and the device structure including various donor–acceptor (D–A) type polymers, additives, thermal treatments, and morphology control. However, there is still an inevitable loss at the interfaces because of the charge transport barriers between the active layer and the metal cathode [14].

To achieve effective charge transport between the interfaces, a number of investigations to study the effects of introducing an interlayer have been recently reported. In particular, most research efforts have focused on alcohol/water-soluble conjugated polymer electrolytes (CPEs) for the interlayer. In the Cao group, a PCE of 8.3% was reported with a device structure that introduced poly [(9,9-bis(30-(*N*,*N*-dimethylamino)propyl)-2,7-fluorene)-alt-2,7-(9,9-dioctylfluorene)] (PFN) between the active layer and the cathode, and an inverted device configuration with PFN improved the PCE to 9.2% with increase in the J_{SC}, V_{OC}, and FF [15,16]. It has been suggested that these interlayers introduce an enhanced built-in potential across the device because of the presence of an interface dipole, which is conducive to refinement in the charge-transport, elimination of the built-up space charge, and diminution in the recombination losses of the charge carriers [14,15].

Small molecules have various advantages compared with polymers, such as straightforward synthesis and purification, monodispersity, precise structures, residual end functionality and good reproducibility [17,18]. A number of research studies on active materials using small molecules have been reported [19–21]; however, only a few investigations of small molecule interlayers produced by solution processing have been reported in the fields of OLEDs and OPVs [4,22]. In the Fang group, a PCE of 9.2% was reported with a small molecule interlayer using an n-type benzothiadiazole derivative in an inverted cell [23]. Recently, we reported a small molecule interlayer using a p-type pyrene derivative with a PCE of 8.3% in an inverted cell [24].

* Corresponding author.
E-mail address: skdlee3@gmail.com (S. Lee).
[1] Tel.: +82 41 589 8551; fax: +82 41 589 8550.

http://dx.doi.org/10.1016/j.solmat.2015.04.042
0927-0248/

In this study, we synthesized alcohol/water-soluble small molecules with various p- and n-type backbones. We introduced various p- and n-type molecules into the backbone to achieve effective charge transfer between the interfaces and ordered orientation. Due to the effective charge transfer and ordered orientation, improved FF, J_{SC}, V_{OC} and PCE values are expected in these OPVs.

2. Experimental section

2.1. Instruments and characterization

Unless otherwise specified, all reactions were performed under a nitrogen atmosphere. The solvents were dried using standard procedures. All column chromatography was performed with silica gel (23–400 mesh, Merck) as the stationary phase. ^{1}H NMR spectra were collected using a Bruker ARX 400 spectrometer on solutions in $CDCl_3$ with chemical concentrations recorded in ppm units using TMS as the internal standard. Elemental analyses were measured using an EA1112 apparatus using a CE Instrument. Electronic absorption spectra were measured in chloroform using an HP Agilent 8453 UV–vis spectrophotometer. The cyclic voltammetric waves were obtained using a Zahner IM6eX electrochemical workstation with a 0.1 M acetonitrile solution (purged with nitrogen for 20 min) containing tetrabutyl ammonium hexafluorophosphate (Bu_4NPF_6) as the electrolyte at a constant scan rate of 50 mV/s. ITO, a Pt wire, and silver/silver chloride [Ag in 0.1 M KCl] were used as the working, counter-, and reference electrodes, respectively. The electrochemical potential was calibrated against Fc/Fc^+. The HOMO levels of the polymers were determined using the oxidation onset value. The onset potentials are defined as the values obtained from the intersection of the two tangents drawn at the rising current and the baseline changing current of the CV curves. TGA measurements were performed on a NETZSCH TG 209 F3 thermogravimetric analyzer. Differential scanning calorimetry (DSC) was used to determine phase transition temperatures on a Netzsch DSC 200 F3 maia differential scanning calorimeter with a constant heating/cooling rate of 10 °C/min. All GPC analyses were performed using THF as an eluent and a polystyrene standard as a reference. Grazing incidence X-ray diffraction (GIXD) patterns were obtained using a SmartLab 3 kW (40 kV, 30 mA, Cu target, wavelength: 1.541871 Å) instrument from Rigaku, Japan. Topographic images of the active layers were obtained through atomic force microscopy (AFM) in tapping mode under ambient conditions using an XE-100 instrument. Scanning Kelvin probe microscopy (SKPM) measurements were carried out on AFM equipment using the standard SKPM mode. Theoretical analyses were performed using density functional theory (DFT) as approximated by the B3 LYP functional and employing the 6-31G* basis set in Gaussian09.

2.2. Fabrication and characterization of polymer solar cells

All of the bulk-heterojunction PV cells were prepared using the following device fabrication procedure. Glass/indium tin oxide (ITO) substrates [Sanyo, Japan (10 Ω/γ)] were sequentially lithographically patterned, cleaned with detergent, and ultrasonicated in deionized water, acetone, and isopropyl alcohol. The substrates were then dried on a hot plate at 120 °C for 10 min and treated with oxygen plasma for 10 min to improve the contact angle immediately before the film coating process. Poly(3,4-ethylenedioxythiophene):poly(styrenesulfonate) (PEDOT:PSS, Baytron P 4083 Bayer AG) was passed through a 0.45-μm filter before being deposited onto the ITO substrates at a thickness of approximately 32 nm by spin coating at 4000 rpm in air and then were dried at 120 °C for 20 min inside a glove box. Composite solutions with polymers and PCBM were prepared using chlorobenzene (CB) with 1,8-diiodooctane (DIO). The concentration was adequately controlled in the 0.3–0.5 wt% range. The solutions were then filtered through a 0.45-μm PTFE filter and spin coated (500–2000 rpm, 30 s) on top of the PEDOT:PSS layer. The PFN solution in methanol and acetic acid was spin coated on the top of the obtained active layer at 4000 rpm for 30 s to form a thin interlayer of 8–10 nm. The device fabrication was completed by depositing thin layers of Al (200 nm) at pressures of less than 10^{-6} Torr. The active area of the device was 4.0 mm^2. Finally, the cell was encapsulated using UV-curing glue (Nagase, Japan). In this study, all of the devices were fabricated with the following structure: ITO glass/PEDOT:PSS/polymer:PCBM/with or without interlayer/Al/encapsulation glass.

The illumination intensity used to test the OPVs was calibrated using a standard Si photodiode detector that was equipped with a KG-5 filter. The output photocurrent was adjusted to match the photocurrent of the Si reference cell to obtain a power density of 100 mW/cm^2. After encapsulation, all of the devices were operated under ambient atmosphere at 25 °C. The current–voltage (I–V) curves of the photovoltaic devices were measured using a computer-controlled Keithley 2400 source measurement unit (SMU) that was equipped with a Peccell solar simulator under an illumination of AM 1.5G (100 mW/cm^2). The thicknesses of the thin films were measured using an ellipsometer of Elli-SE=Uam12.

2.3. Materials

All reagents were purchased from Aldrich, Acros or TCI. All chemicals were used without further purification. PTB7 was purchased from Nano clean tech (Product no.: OS0737). The following compounds were synthesized following modified literature procedures: *N*,*N*-dimethyl-3-(4-(4,4,5,5-tetramethyl-1,3,2-dioxaborolan-2-yl)phenoxy)propan-1-amine [24], 2,9-dibromo-5,12-bis(2-octyldodecyl)quinolino[2,3-b]acridine-7,14(5H,12H)-dione [6], and 3,6-bis(5-bromothiophen-2-yl)-2,5-bis(2-hexyldecyl)pyrrolo[3,4-c]pyrrole-1,4(2H,5H)-dione [25].

2.3.1. 2,7-dibromo-11,12-bis(octyloxy)dibenzo[a,c]phenazine

Under a nitrogen atmosphere, 4,5-bis(octyloxy)benzene-1,2-diamine (1 g, 2.73 mmol) and 2,7-dibromophenanthrene-9,10-dione (1.43 g, 3.27 mmol) were dissolved in 20 ml ethanol and 0.1 ml acetic acid. The mixture was refluxed for 24 h at 85 °C. After cooling to room temperature, the reaction mixture was washed with a $NaHCO_3$ solution. The reaction mixture was purified by column chromatography on silica gel (dichloromethane as eluent) to obtain the product as a green solid (0.96 g, yield: 50.5%). ^{1}H NMR (400 MHz; $CDCl_3$; Me_4Si): 9.14 (s, 2H), 8.12 (d, 2H), 7.67 (dd, 2H), 4.21 (t, 4H), 1.98(t, 4H), 1.40(m, 20H), 0.92(t, 6H). Anal. Calcd for: $C_{36}H_{42}Br_2N_2O_2$: C, 62.26; H, 6.10; N, 4.03; O, 4.61. Found: C, 61.65; H, 5.97; N, 3.92; O, 6.02.

2.3.2. 3,3′-(4,4′-(11,12-bis(octyloxy)dibenzo[a,c]phenazine-2,7-diyl) bis(4,1-phenylene))bis(oxy)bis(N,N-dimethylpropan-1-amine) (BPA)

M1 (0.39 g, 1.29 mmol), M2 (0.30 g, 0.43 mmol) and $Pd(PPh_3)_4$(0) (0.09 g, 0.08 mmol) were placed in a Schlenk tube and purged with three nitrogen/vacuum cycles. Under nitrogen atmosphere, 2 M degassed aqueous K_2CO_3 (10 mL) and dry 1,4-dioxane (20 mL) were added. The mixture was heated to 90 °C and stirred in dark for 48 h. After reaction quenching, the mixture was poured into 50 mL water and extracted with $CHCl_3$ (100 mL). The combined organic layers were washed with brine and dried over anhydrous $MgSO_4$. The solvent was removed by rotary evaporation, and the final product was obtained after vacuum drying. A yellowish-green solid was obtained (0.34 g, yield: 88%). ^{1}H NMR (400 MHz; $CDCl_3$; Me_4Si): δ=9.40 (s, 2H), 8.43 (d, 2H), 7.83 (d, 2H), 7.75 (d, 4H), 7.41 (s, 2H), 7.00 (d, 4H), 4.17 (t, 4H), 4.03 (t, 4H), 2.43 (t, 4H), 2.22 (s, 12H), 1.93 (m, 8H), 1.49 (m, 4H), 1.31 (m, 16H), 0.83 (m, 6H). ^{13}C NMR (100 MHz; $CDCl_3$;

Me_4Si): 158.82; 153.22; 140.09; 139.80; 139.47; 133.17; 130.67; 129.65; 128.35; 127.60; 123.27; 122.90; 114.87; 106.80; 69.18; 66.38; 56.49; 45.61; 31.87; 29.43; 29.33; 28.95; 27.69; 26.12; 22.72; 14.15. Anal. Calcd for: $C_{58}H_{74}N_4O_4$: C, 78.16; H, 8.37; N, 6.29; O, 7.18. Found: C, 75.05; H, 8.29; N, 4.13; O, 6.61.

2.3.3. 2,9-bis(4-(3-(dimethylamino)propoxy)phenyl)-5,12-bis(2-octyldodecyl)quinolino[2,3-b]acridine-7,14(5H,12H)-dione (QA)

M1 (0.26 g, 0.87 mmol), M3 (0.30 g, 0.29 mmol) and $Pd(PPh_3)_4(0)$ (0.06 g, 0.05 mmol) were placed in a Schlenk tube and purged with three nitrogen/vacuum cycles. Under nitrogen atmosphere, 2 M degassed aqueous K_2CO_3 (10 mL) and dry 1,4-dioxane (20 mL) were added. The mixture was heated to 90 °C and stirred in dark for 48 h. After reaction quenching, the mixture was poured into 50 mL water and extracted with $CHCl_3$ (100 mL). The combined organic layers were washed with brine and dried over anhydrous $MgSO_4$. The solvent was removed by rotary evaporation, and the final product was obtained after drying in vacuum. An orange solid was obtained (0.29 g, yield: 79%). ^{1}H NMR (400 MHz; $CDCl_3$; Me_4Si): δ=8.84 (s, 2H), 8.76 (s, 2H), 7.93 (s, 2H), 7.65 (d, 4H), 7.59 (s, 2H), 7.03 (d, 4H), 4.53 (s, 4H), 4.10 (t, 4H), 2.50 (t, 4H), 2.27 (s, 14H), 2.01 (m, 4H), 1.43-1.18 (m, 72H), 0.83 (t, 12H). ^{13}C NMR (100 MHz; $CDCl_3$; Me_4Si): 177.99; 158.66; 141.68; 136.08; 133.02; 132.63; 131.87; 128.95; 127.73; 127.32; 126.74; 125.91; 124.67; 121.31; 116.01; 114.95; 114.40; 66.35; 56.45; 49.93; 45.56; 36.87; 31.90; 31.84; 31.74; 29.99; 29.63; 29.60; 29.52; 29.47; 29.34; 29.28; 27.61; 26.67; 22.68; 22.64; 14.12; 14.09. Anal. Calcd for: $C_{82}H_{122}N_4O_4$: C, 80.21; H, 10.01; N, 4.56; O, 5.21. Found: C, 79.54; H, 9.96; N, 2.06; O, 5.41.

2.3.4. 3,6-bis(5-(4-(3-(dimethylamino)propoxy)phenyl)thiophen-2-yl)-2,5-bis(2-hexyldecyl)pyrrolo[3,4-c]pyrrole-1,4(2H,5H)-dione (DPPA)

M1 (0.30 g, 0.99 mmol), M4 (0.30 g, 0.33 mmol) and $Pd(PPh_3)_4(0)$ (0.07 g, 0.06 mmol) were placed in a Schlenk tube and purged with three nitrogen/vacuum cycles. Under nitrogen atmosphere, 2 M degassed aqueous K_2CO_3 (10 mL) and dry 1,4-dioxane (20 mL) were added. The mixture was heated to 90 °C and stirred in dark for 48 h. After reaction quenching, the mixture was poured into 50 mL water and extracted with $CHCl_3$ (100 mL). The combined organic layers were washed with brine and dried over anhydrous $MgSO_4$. The solvent was removed by rotary evaporation, and the final product was obtained after drying in vacuum. A dark purple solid was obtained (0.31 g, yield: 84%). ^{1}H NMR (400 MHz; $CDCl_3$; Me_4Si): δ=8.93 (d, 2H), 7.60 (d, 4H), 7.34 (d, 2H), 6.95 (d, 4H), 4.06 (t, 8H), 2.48 (t, 4H), 2.31 (s, 12H), 1.99 (m, 6H), 1.33-1.21 (m, 48H), 0.83 (m, 12H). ^{13}C NMR (100 MHz; $CDCl_3$; Me_4Si): 161.74; 159.69; 149.76; 139.71; 136.83; 127.86; 127.42; 125.92; 123.32; 115.07; 107.88; 66.37; 56.31; 46.26; 45.53; 37.90; 31.91; 31.84; 31.35; 30.08; 29.74; 29.59; 29.32; 27.48; 26.40; 26.37; 22.68; 22.64; 14.13. Anal. Calcd for: $C_{68}H_{102}N_4O_4S_2$: C, 74.00; H, 9.32; N, 5.08; S, 5.81; O, 5.80. Found: C, 70.57; H, 9.07; N, 2.50; S, 5.29; O, 5.26.

3. Results and discussion

3.1. Synthesis and thermal properties

Scheme 1 shows the chemical structures of the materials and the synthesis process. As shown in Scheme 1, BPA, QA and DPPA were synthesized by a Suzuki-coupling reaction with the monomers M1, M2, M3 and M4. The reaction mixtures were heated for 48 h at 110 °C with a palladium(0) catalysts and a 2 M potassium carbonate solution in 1,4-dioxane as a solvent. The synthesized BPA, QA and DPPA were purified using several rounds of re-crystallization with methanol/H_2O. The yields of BPA, QA and DPPA were 88%, 79%, and 84%, respectively. The obtained BPA, QA and DPPA were soluble in organic solvents (chlorobenzene, ortho-dichlorobenzene, and chloro form) and highly polar solvents (methanol and ethanol).

The solubilities of BPA, QA, and DPPA in methanol were investigated. Acetic acid was added to methanol to improve the solubility relative to the protonation of the terminal dimethylamino groups. For the same weight ratio (5 mg of material/co-solvent (10 μL acetic acid + 2.5 mL MeOH)), BPA and QA were soluble with heat treatment; however, DPPA completely dissolves without heat treatment at RT.

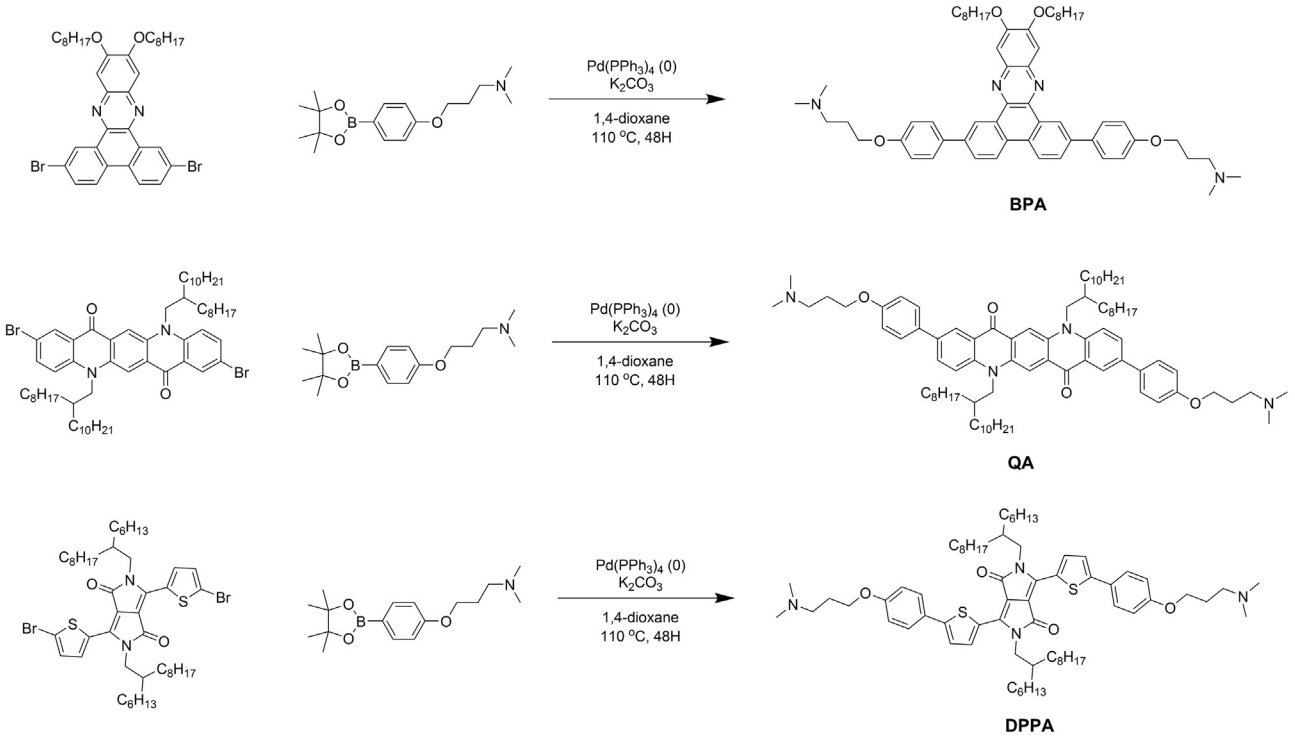

Scheme 1. Synthesis route of BPA, QA, and DPPA.

Table 1
Optical and electrochemical properties of all the molecules.

Molecules	Absorption, λ_{max} (nm)		E_{ox}^{onset}(V)	E_{HOMO} (eV)[c]	E_{LUMO} (eV)[d]	E_{opt} (eV)[e]	Absorption coefficient
	Solution[a]	Film[b]					
BPA	323, 394, 416	322, 394, 416	1.32	−5.65	−2.89[d]	2.89	$3.7*10^{-4}$
QA	330, 547	319, 539	1.05	−5.38	−3.17[d]	2.21	$8.3*10^{-4}$
DPPA	334, 407, 564, 592	337, 426, 568, 633	0.80	−5.13	−3.31[d] −3.49[f]	1.82	$3.7*10^{-4}$

[a] Absorption spectrum in $CHCl_3$ solution (10^{-6} M).
[b] Spin-coated thin film (50 nm).
[c] Calculated from the oxidation onset potentials under the assumption that the absolute energy level of Fc/Fc+ was −4.8 eV below a vacuum.
[d] HOMO − E_{opt}.
[e] Calculated from the redox onset potentials under the assumption that the absolute energy level of Fc/Fc+ was −4.8 eV below a vacuum.
[f] Estimated from the onset of UV–vis absorption data of the thin film.

Thus, DPPA exhibited higher solubility in highly polar solvents compared with BPA and QA, which was due to the rigid backbones of BPA and QA. Using BPA, QA, and DPPA solutions, uniform and semi-transparent films were formed by spin coating.

Table 1 shows the thermal properties of all of the synthesized molecules. BPA, QA, and DPPA experienced 5% weight loss at temperatures of 344, 381 and 353 °C, respectively. This result was similar to the thermal stability of a conjugated polymer, indicating that all of these molecules are applicable to OLED and OPVs, which demand a thermal stability above 300 °C [6]. In particular, the degradation of QA was 28–37 °C higher than that of BPA and DPPA, which may be due to the high stability of the quinacridone derivative.

We investigated the thermal phenomena using differential scanning calorimetry (DSC) (Fig. S2). The DSC thermograms of QA and DPPA revealed no obvious liquid-crystal phase transitions and exhibited only melting to an isotropic phase upon heating at 138 and 124 °C, respectively. In contrast, BPA exhibited an obvious liquid-crystal phase with a smectic phase upon heating at 229 °C.

3.2. Optical and electrochemical properties

Fig. 1(a) and (b) shows the UV–visible spectra of all the molecules. The maximum absorption peaks of BPA (λ_{max}) were observed at 394 and 416 nm in solution (10^{-5} M in a co-solvent of acetic acid and methanol) and at 394 and 416 nm in the thin film. Notably, the absorption spectrum of the BPA thin film approximately matched that of the solution, which indicates that the more planar phenazine unit effectively decreased the steric hindrance in the thin film and facilitated stronger association in solution [26].

The maximum absorption peaks of QA (λ_{max}) were found at 330 and 547 nm in solution and at 319 and 539 nm in the thin film. The QA film spectrum was blue-shifted compared with the solution spectrum, which was caused by the π–π* transition distribution between quinacridone chains, whereas the quinacridone derivative formed the film [27].

The maximum absorption peaks of DPPA (λ_{max}) occurred at 334, 407, 564, and 592 nm in solution and at 337, 426, 568, and 633 nm in the thin film. The DPPA film spectrum was red-shifted compared with the solution spectrum, which was explained by much more planar molecular conformations in the solid state [28]. Interestingly, the DPPA film showed a strong shoulder peak at approximately 633 nm compared with the DPPA solution, which was due to the ordered orientation of DPPA [29]. In this regard, additional interpretation will be provided in the discussion of the XRD data.

Fig. 1(c) shows the UV–vis spectra of ITO/PEDOT:PSS/PTB7:PCBM/without or with interlayer. The absorption spectra of the structures with BPA and QA were similar to the absorption spectrum of the structure without an interlayer. In contrast, the absorption spectrum of the structure with DPPA showed increased intensity compared with that without an interlayer. These results may be due to energy transfer between the active layer and the DPPA interlayer, which is expected to improve the photocurrent in OPV devices [23].

The calculated optical band gaps of BPA, QA, and DPPA from the measured value of UV onset for the films were 2.89, 2.21, and 1.82 eV, respectively.

Fig. 2 shows the cyclic voltammograms of all of the molecules. The cyclic voltammograms were recorded in a 0.1 M tetrabutylammonium–hexafluorophosphate acetonitrile solution. As shown in Fig. 2, BPA and QA exhibited typical p-type oxidation peaks. The oxidation (E_{ox}^{onset}) of BPA and QA occurred at +1.32 V and 1.05 V, respectively, and the HOMO energy levels of BPA and QA determined through calculation were −5.65 eV and −5.38 eV, respectively. The LUMO energy levels were obtained from the gap between the HOMO energy levels and the optical band gap energies. As a result, the LUMO levels of BPA and QA were −2.89 and −3.17 eV, respectively. In the case of BPA, high oxidation stability may be expected due to its low HOMO energy level.

In contrast, DPPA exhibited typical n-type oxidation and reduction peaks. The oxidation (E_{ox}^{onset}) and reduction (E_{red}^{onset}) of DPPA occurred at +0.80 V and −0.80 V, respectively, and the HOMO and LUMO energy levels of DPPA determined through calculation were −5.13 and −3.49 eV, respectively. As shown in the band diagram in Fig. 2(b), the DPPA LUMO level (−3.31 eV) was similar to that of PTB7 (−3.31 eV), which can be appropriate as an electron transport layer in inverted OPV cells. In addition, the DPPA LUMO level (−3.31 eV) was the lowest of the synthesized molecules, which suggests that electron charge transport can occur from DPPA to the Al electrode.

3.3. XRD analysis and DFT calculation

Fig. 3 shows the X-ray diffraction investigation of the films of all of the molecules to analyze their ordering structures. The samples for measurement were fabricated as spin casted films on the surface of Si-wafers using solutions containing acetic acid and MeOH.

In the out-of-plane diffraction pattern of QA, as shown in Fig. 3, sharp diffraction peaks occurred at 3.5° and 5.7°, which indicates the formation of an ordered structure as an out-of-plane peak (100) due to the alkyl side chain of quinacridone. In addition, a prominent diffraction peak occurred at 17.7°, which indicates an out-of-plane peak (010) due to the molecular packing by π–π stacking. The π–π stacking distance of QA was 0.50 nm ($\lambda=2d\sin\theta$). The diffraction peaks of DPPA were similar to QA. In the out-of-plane diffraction pattern of DPPA, sharp diffraction peaks occurred at 4.9°, which indicates the formation of an ordered structure as an out-of-plane peak (100) due to the alkyl side chain of the DPP derivative. In addition, a prominent diffraction peak occurred at 20.1°, which

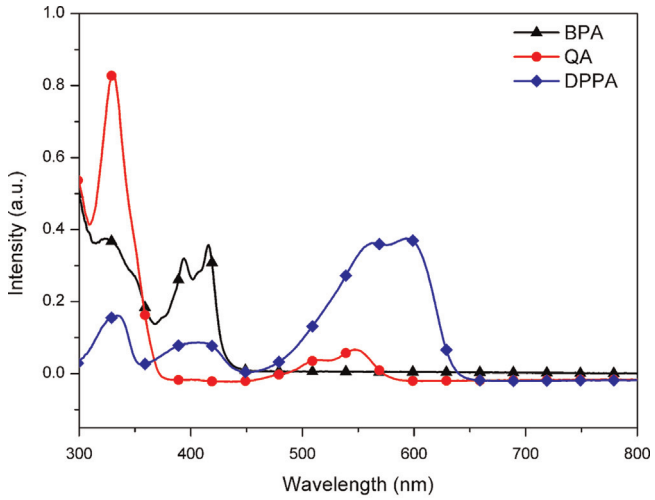

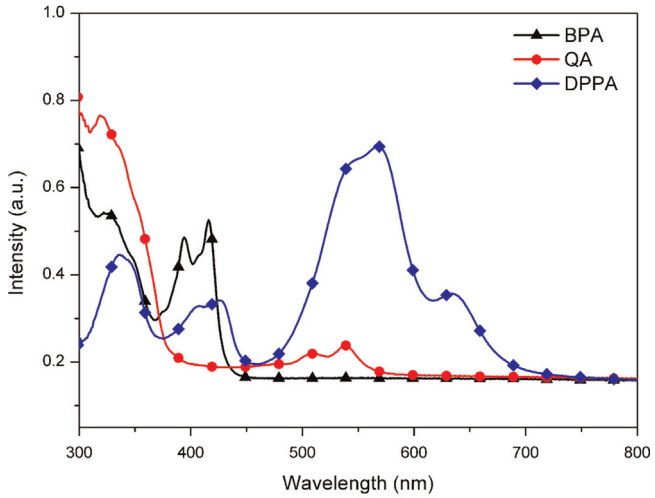

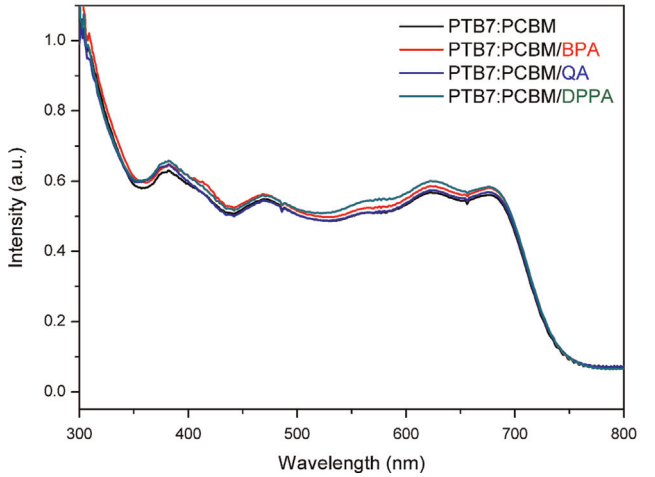

Fig. 1. Absorption spectra for all molecules in (a) solution and (b) thin film (c) spin-coated layers of all molecules on the top of the active layer (PTB7:$PC_{71}BM$).

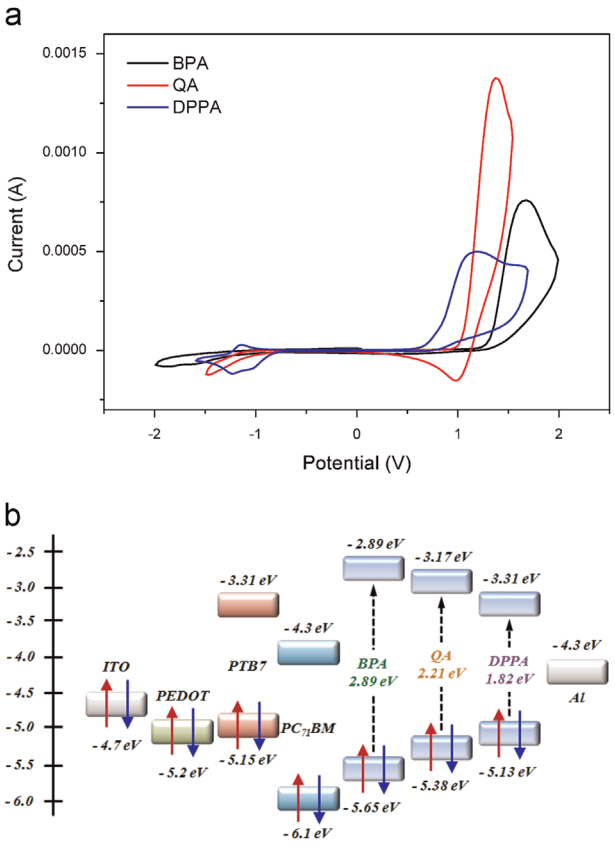

Fig. 2. (a) Cyclic voltammogram of all molecules (b) band diagram of all molecules, ITO, $PC_{71}BM$, and Al.

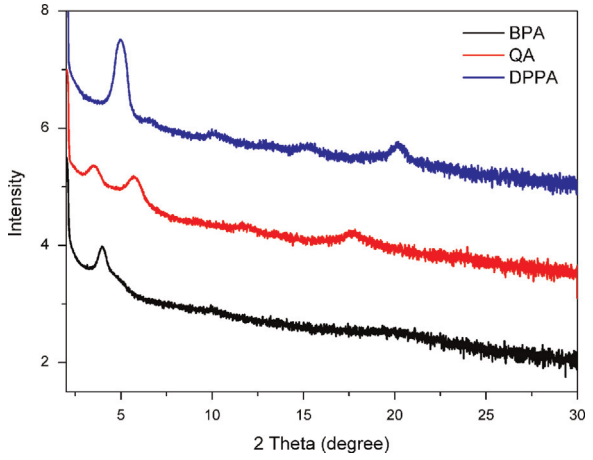

Fig. 3. X-ray diffraction pattern in thin films of all molecules (out-of-plane).

indicates an out-of-plane peak (010) due to the molecular packing by π–π stacking. The π–π stacking distance of DPPA was 0.44 nm. In contrast, BPA exhibited a different diffraction peak compared with QA and DPPA. In the out-of-plane diffraction pattern of DPPA, sharp diffraction peaks occurred at 3.9°, and a diffraction peak corresponding to π–π stacking was rarely observed. The diffraction peaks of QA and DPPA were sharper compared with that of BPA, which indicates that QA and DPPA exhibited a more strongly ordered orientation than BPA. Based on this result, in the case of QA and DPPA, it is expected that the series and shunt resistance of the OPV device would decrease due to the ordered orientation.

The torsion angles were comparatively analyzed by calculating all of the compounds using a DFT calculation. For BPA, the torsion angle between phenazine and benzene was 35°, and for QA, the torsion angle between quinacridone and benzene was 33–34°. In contrast, the torsion angle between thiophene and benzene for DPPA was 24–27°. Compared with QA, the formation of a planar backbone was observed for DPPA (see SI), which suggests that stronger π–π stacking interactions occur in DPPA. This result was confirmed by the aforementioned XRD results. As shown in the XRD results, the π–π stacking distance of DPPA (0.44 nm) was lower than that of QA (0.50 nm).

3.4. Characterization of OPV devices

Fig. 4 and Table 2 show the data for device performance. Each device was fabricated as follows: ITO (170 nm)/PEDOT:PSS (40 nm)/active layer (50–80 nm)/interlayer (~8 nm)/Al (100 nm). The donor polymer in the active layer was thieno[3,4-b]-thiophene-benzodithiophene (PTB7), and the acceptor derivative in the active layer was phenyl-C71-butyric acid methyl ester ($PC_{71}BM$). The blend ratio for PTB7/$PC_{71}BM$ was 1:1.5 by weight, and the active layer was spin coated from a mixed solvent (chlorobenzene 97 vol%, 1,8-diiodoctane 3 vol%). A film of the interlayer solution (BPA, QA, DPPA) was formed on top of the active layer (thickness of 8 nm) using spin coating. An Al electrode (100 nm) was deposited on top by evaporation through a shadow mask. More than 100 devices were fabricated to confirm device reproducibility. The OPV device without an interlayer exhibited V_{OC} of 0.59 V, J_{SC} of 14.6 mA/cm^2, FF of 55.8% and PCE of 4.9%, which is similar to the results of a PTB7 device reported in the literature [15,30].

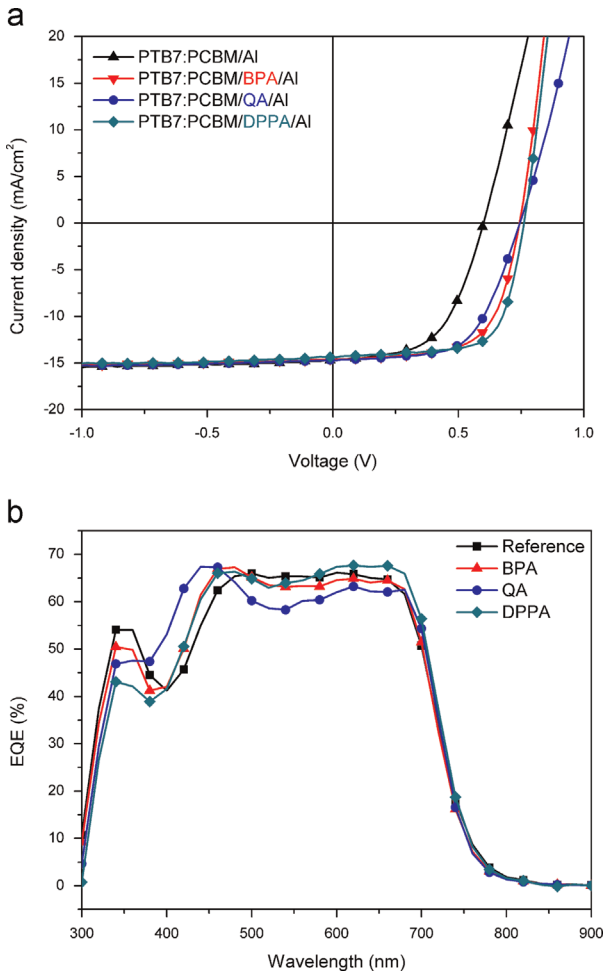

Fig. 4. (a) *J–V* characteristics (b) EQE spectra of the BHJ solar cells with the device. (Conventional device structure: ITO/PEDOT:PSS/ PTB7:$PC_{71}BM$(1:1.5)/without or with interlayer/Al.)

For a device with BPA, the V_{OC}, J_{SC}, FF and PCE were 0.73 V, 14.6 mA/cm^2, 63.2% and 6.6%, respectively. For a device with QA, the V_{OC}, J_{SC}, FF and PCE were 0.75 V, 14.4 mA/cm^2, 69.7% and 7.6%, respectively. For a device with DPPA, the V_{OC}, J_{SC}, FF and PCE were 0.75 V, 15.1 mA/cm^2, 69.0% and 7.9%, respectively. To investigate the influence of the solvent treatment (acetic acid and methanol) on the active layer, another type of control device was also fabricated. The device with only solvent showed slightly improved properties (V_{OC} of 0.61 V, J_{SC} of 14.5 mA/cm^2, FF of 56.6% and PCE of 5.1%). However, the device with only solvent did not exhibit drastically improved properties compared with the device with interlayers. This result suggests that an interlayer of various molecules leads to additional benefits that improve charge extraction.

All the devices with an interlayer (BPA, QA, or DPPA) exhibited substantially increased FF values compared with the device without an interlayer. In particular, the FF values of the devices with QA and DPPA (69.7% and 69.0%, respectively) were higher than that with BPA (63.2%), which resulted in the improved PCE of the devices with QA and DPPA (QA 7.6%, DPPA 7.9% vs. BPA 6.6%). The series resistances for the devices with QA and DPPA, as shown in Table 2, were 6.1 Ω/cm^2 and 5.2 Ω/cm^2, respectively, and the series resistance for the device with BPA was 12.3 Ω/cm^2, i.e., the series resistances of the QA and DPPA layers were lower compared with the BPA layer. This reduction of series resistance could increase the FF. Thus, the device with QA and DPPA exhibited higher FF than that of BPA because of the decreased series resistance resulting from the ordered orientation and packing of QA and DPPA [6,18].

For the device containing a PBPA derivative with tetra-amine previously reported in our group, the V_{OC}, J_{SC}, FF and PCE were 0.73 V, 14.6 mA/cm^2, 65.1% and 7.0%, respectively [24]. Despite increased amine derivatives, the device containing PBPA did not show improved performance compared with the device containing DPPA and QA. This result suggests that the increased number of amines does not lead to improved properties.

To confirm the precision of the cell performances, the external quantum efficiency (EQE) of each device was investigated. The EQE curves are shown in Fig. 4(b). The short-circuit current density for the BPA, QA, and DPPA devices obtained from the EQE data were 13.6, 13.7, and 14.1 mA/cm^2, respectively. Although it forms a slight gap, the EQE data are similar to the cell current-density of the AM 1.5 condition. The EQE results were similar to the UV spectra results in Fig. 1(a). The EQE of the devices containing BPA and QA exhibited strong intensities at approximately 400–500 nm, whereas the EQE of the device containing DPPA exhibited a strong intensity at approximately 550–700 nm. The current density of DPPA showed a slightly higher value compared with that of BPA and QA. This result was caused by energy transfer between the active layer and the DPPA interlayer, as shown in the UV spectra (Fig. 1(c)).

To investigate the oxidative stability of photovoltaic devices based on molecules (BPA, QA, DPPA), the current density–voltage

Table 2
Photovoltaic performance of the BHJ solar cells.

Device structure	V_{OC} (V)	J_{SC} (mA/cm^2)	FF (%)	PCE (%)	R_s (Ω/cm^2)	R_{sh} (Ω/cm^2)
Al	0.59	14.6	55.8	4.9 (4.9)[b]	10.8	404
Solvent/Al	0.61	14.5	56.6	5.1 (5.0)[b]	8.9	403
PBPA/Al[a]	0.73	14.6	65.1	7.0 (6.9)[b]	6.9	1044
BPA/Al[a]	0.73	14.7	63.2	6.6 (6.6)[b]	12.3	1111
QA/Al[a]	0.75	14.4	69.7	7.6 (7.5)[b]	6.1	758
DPPA/Al[a]	0.75	15.1	69.0	7.9 (7.8)[b]	5.2	1058

[a] Conventional device structure: ITO/PEDOT:PSS/PTB7:$PC_{71}BM$(1:1.5)/without or with interlayer/Al.
[b] Average PCE value for five devices.

(*J–V*) curves of the devices were measured under ambient conditions for half month. All the devices were encapsulated to prevent oxidation of the metal electrode and maintained under ambient conditions. As shown in Fig. S4, the PCE values of the devices based on the QA and DPPA had changed slightly after one day. Moreover, the PCE values of these devices decreased by only approximately 25–27% after half-month, which is likely due to the electrochemical stability.

3.5. Morphology analysis

To analyze the topology of the interlayer, atomic force microscopy (AFM) was investigated (Fig. 5). As shown in Fig. 5(a), a smooth morphology was observed between PTB7 and $PC_{71}BM$ with a roughness of 0.9 nm. For all of the interlayer films on top of the PTB7:$PC_{71}BM$ blend film (Fig. 5(b)–(d)), large island-domains were observed. The roughnesses of all of the interlayer films were 1.7–1.8 nm. In the case of the PFN film on top of the PTB7:$PC_{71}BM$ blend film, a number of raised island-domains were distributed over the film, which was similar to the morphology of the interlayer films, with an increased roughness of 2.3 nm [24]. The roughnesses of all the interlayer films (BPA, QA, and DPPA) were lower than that of PFN. All the molecules (BPA, QA, and DPPA) were assumed to form flat and ordered packing due to their planar structures, which may lead to a lower roughness compared with the packing of the PFN film. In contrast, in the case of the PFN film, the PFN derivatives were assumed to exhibit some aggregation, which may lead to increased roughness [14]. Thus, the interlayer films (BPA, QA, and DPPA) reduced the interfacial resistance compared with that of the PFN film due to their decreased roughnesses, which led to the improved FF of the devices containing interlayer films (BPA, QA, and DPPA) [31].

4. Conclusions

In this study, we synthesized novel alcohol/water-soluble small molecules with p- and n-type derivatives (BPA, QA, and DPPA) using a simple synthesis process. The synthesized molecules exhibited good thermal stability and high solubility for organic and polar solvents. According to the CV measurements, the LUMO level of DPPA (− 3.49 eV) was similar to that of PTB7 (− 3.31 eV), indicating that DPPA can be appropriate as an electron transport layer in an inverted OPV cell. According to XRD measurements, the diffraction peaks of QA and DPPA were sharper compared with that of BPA, which indicates that QA and DPPA exhibited a more strongly ordered orientation than BPA. The OPV device using DPPA exhibited improved characteristics compared with the devices without an interlayer (FF 69.0% vs. 55.8%, PCE 7.9% vs. 4.9%) due to the reduction of the interfacial resistance and ordered orientation. All the molecules (BPA, QA, and DPPA) were assumed to form flat

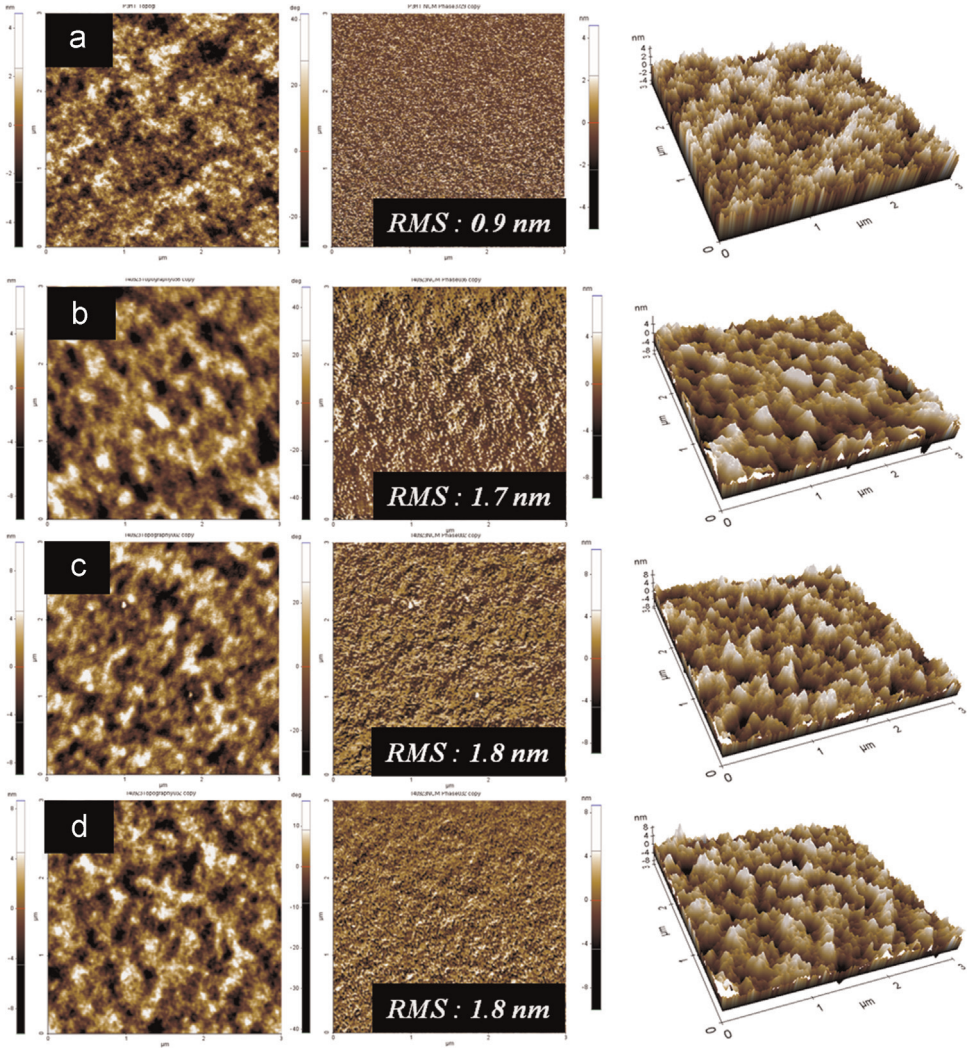

Fig. 5. Topographic AFM images of (a) PTB7:$PC_{71}BM$ film, (b) PTB7:$PC_{71}BM$/BPA film, (c) PTB7:$PC_{71}BM$/QA film and (d) PTB7:$PC_{71}BM$/DPPA film ($3 \times 3\ \mu m^2$).

and ordered packing due to their planar structures, which may lead to a lower roughness compared with the packing of a PFN film.

Acknowledgments

This work was supported by the New & Renewable Energy Core Technology Program of the Korea Insitute of Energy Technology Evaluation and Planning (KETEP) grant funded by the Ministry of Trade, Industry and Energy (MI, Korea) (No. 20133030000180).

Appendix A. Supplementary material

Supplementary data associated with this article can be found in the online version at http://dx.doi.org/10.1016/j.solmat.2015.04.042.

References

[1] S. Reineke, F. Lindner, G. Schwartz, N. Seidler, K. Walzer, B. Lussem, K. Leo, White organic light-emitting diodes with fluorescent tube efficiency, Nature 459 (2009) 234–238.
[2] H. Wu, L. Ying, W. Yang, Y. Cao, Progress and perspective of polymer white light-emitting devices and materials, Chem. Soc. Rev. 38 (2009) 3391–3400.
[3] T. Earmme, E. Ahmed, S.A. Jenekhe, Solution-processed highly efficient blue phosphorescent polymer light-emitting diodes enabled by a new electron transport material, Adv. Mater. 22 (2010) 4744–4748.
[4] M.C. Gather, A. Köhnen, K. Meerholz, White organic light-emitting diodes, Adv. Mater. 23 (2011) 233–248.
[5] J. Kuwabara, Y. Nohara, S.J. Choi, Y. Fujinami, W. Lu, K. Yoshimura, J. Oguma, K. Suenobu, T. Kanbara, Direct arylation polycondensation for the synthesis of bithiophene-based alternating copolymers, Polym. Chem. 4 (2013) 947–953.
[6] H.-J. Song, D.-H. Kim, E.-J. Lee, S.-W. Heo, J.-Y. Lee, D.-K. Moon, Conjugated polymer consisting of quinacridone and benzothiadiazole as donor materials for organic photovoltaics: coplanar property of polymer backbone, Macromolecules 45 (2012) 7815–7822.
[7] F.C. Krebs, Fabrication and processing of polymer solar cells: a review of printing and coating techniques, Sol. Energy Mater. Sol. Cells 93 (2009) 394–412.
[8] J.-M. Jiang, P.-A. Yang, T.-H. Hsieh, K.-H. Wei, Crystalline low-band gap polymers comprising thiophene and 2,1,3-benzooxadiazole units for bulk heterojunction solar cells, Macromolecules 44 (2011) 9155–9163.
[9] M. Jørgensen, J.E. Carlé, R.R. Søndergaard, M. Lauritzen, N.A. Dagnæs-Hansen, S.L. Byskov, T.R. Andersen, T.T. Larsen-Olsen, A.P.L. Böttiger, B. Andreasen, L. Fu, L. Zuo, Y. Liu, E. Bundgaard, X. Zhan, H. Chen, F.C. Krebs, The state of organic solar cells—a meta analysis, Sol. Energy Mater. Sol. Cells 119 (2013) 84–93.
[10] Y. Liu, T.T. Larsen-Olsen, X. Zhao, B. Andreasen, R.R. Søndergaard, M. Helgesen, K. Norrman, M. Jørgensen, F.C. Krebs, X. Zhan, All polymer photovoltaics: from small inverted devices to large roll-to-roll coated and printed solar cells, Sol. Energy Mater. Sol. Cells 112 (2013) 157–162.
[11] L. Huo, S. Zhang, X. Guo, F. Xu, Y. Li, J. Hou, Replacing alkoxy groups with alkylthienyl groups: a feasible approach to improve the properties of photovoltaic polymers, Angew. Chem. Int. Ed. 50 (2011) 9697–9702.
[12] S. Dong, C. Bao, H. Tian, D. Yan, Y. Geng, F. Wang, A.B.A.B. – symmetric tetraalkyl titanyl phthalocyanines for solution processed organic field-effect transistors with mobility approaching 1 $cm^2 V^{-1} s^{-1}$, Adv. Mater. 25 (2013) 1165–1169.
[13] X. Feng, V. Marcon, W. Pisula, M.R. Hansen, J. Kirkpatrick, F. Grozema, D. Andrienko, K. Kremer, K. Mullen, Towards high charge-carrier mobilities by rational design of the shape and periphery of discotics, Nat. Mater. 8 (2009) 421–426.
[14] Y. Chen, Z. Jiang, M. Gao, S.E. Watkins, P. Lu, H. Wang, X. Chen, Efficiency enhancement for bulk heterojunction photovoltaic cells via incorporation of alcohol soluble conjugated polymer interlayer, Appl. Phys. Lett. 100 (2012) 203304.
[15] Z. He, C. Zhong, X. Huang, W.-Y. Wong, H. Wu, L. Chen, S. Su, Y. Cao, Simultaneous enhancement of open-circuit voltage, short-circuit current density, and fill factor in polymer solar cells, Adv. Mater. 23 (2011) 4636–4643.
[16] Z. He, C. Zhong, S. Su, M. Xu, H. Wu, Y. Cao, Enhanced power-conversion efficiency in polymer solar cells using an inverted device structure, Nat. Photonics 6 (2012) 591–595.
[17] Z. Li, G. He, X. Wan, Y. Liu, J. Zhou, G. Long, Y. Zuo, M. Zhang, Y. Chen, Solution processable rhodanine-based small molecule organic photovoltaic cells with a power conversion efficiency of 6.1%, Adv. Energy Mater. 2 (2012) 74–77.
[18] O.P. Lee, A.T. Yiu, P.M. Beaujuge, C.H. Woo, T.W. Holcombe, J.E. Millstone, J. D. Douglas, M.S. Chen, J.M.J. Fréchet, Efficient small molecule bulk heterojunction solar cells with high fill factors via pyrene-directed molecular self-assembly, Adv. Mater. 23 (2011) 5359–5363.
[19] Y. Liu, X. Wan, F. Wang, J. Zhou, G. Long, J. Tian, Y. Chen, High-performance solar cells using a solution-processed small molecule containing benzodithiophene unit, Adv. Mater. 23 (2011) 5387–5391.
[20] A.K.K. Kyaw, D.H. Wang, V. Gupta, J. Zhang, S. Chand, G.C. Bazan, A.J. Heeger, Efficient solution-processed small-molecule solar cells with inverted structure, Adv. Mater. 25 (2013) 2397–2402.
[21] B. Walker, C. Kim, T.-Q. Nguyen, Small molecule solution-processed bulk heterojunction solar cells, Chem. Mater. 23 (2010) 470–482.
[22] T.V. Pho, H. Kim, J.H. Seo, A.J. Heeger, F. Wudl, Quinacridone-based electron transport layers for enhanced performance in bulk-heterojunction solar cells, Adv. Funct. Mater. 21 (2011) 4338–4341.
[23] W. Zhang, Y. Wu, Q. Bao, F. Gao, J. Fang, Morphological control for highly efficient inverted polymer solar cells via the backbone design of cathode interlayer materials, Adv. Energy Mater. 4 (2014) 1400359.
[24] H.J. Song, E.J. Lee, D.H. Kim, T.H. Lee, M. Goh, S. Lee, D.K. Moon, Solution-processed interlayer of discotic-based small molecules for organic photovoltaic devices: enhancement of both the open-circuit voltage and the fill factor, Dyes Pigment. 113 (2015) 210–218.
[25] Z. Zeng, Y. Li, J. Deng, Q. Huang, Q. Peng, Synthesis and photovoltaic performance of low band gap copolymers based on diketopyrrolopyrrole and tetrathienoacene with different conjugated bridges, J. Mater. Chem. A 2 (2014) 653–662.
[26] Y. Zhang, J. Zou, H.-L. Yip, K.-S. Chen, D.F. Zeigler, Y. Sun, A.K.Y. Jen, Indacenodithiophene and quinoxaline-based conjugated polymers for highly efficient polymer solar cells, Chem. Mater. 23 (2011) 2289–2291.
[27] D. Neher, Polyfluorene homopolymers: conjugated liquid-crystalline polymers for bright blue emission and polarized electroluminescence, Macromol. Rapid Commun. 22 (2001) 1365–1385.
[28] H.-J. Song, D.-H. Kim, E.-J. Lee, D.-K. Moon, Conjugated polymers consisting of quinacridone and quinoxaline as donor materials for organic photovoltaics: orientation and charge transfer properties of polymers formed by phenyl structures with a quinoxaline derivative, J. Mater. Chem. A 1 (2013) 6010–6020.
[29] Y. Li, J. Zou, H.-L. Yip, C.-Z. Li, Y. Zhang, C.-C. Chueh, J. Intemann, Y. Xu, P.-W. Liang, Y. Chen, A.K.Y. Jen, Side-chain effect on cyclopentadithiophene/fluorobenzothiadiazole-based low band gap polymers and their applications for polymer solar cells, Macromolecules 46 (2013) 5497–5503.
[30] B.A. Collins, Z. Li, J.R. Tumbleston, E. Gann, C.R. McNeill, H. Ade, Absolute measurement of domain composition and nanoscale size distribution explains performance in PTB7:$PC_{71}BM$ solar cells, Adv. Energy Mater. 3 (2013) 65–74.
[31] Y.-M. Chang, C.-Y. Leu, Conjugated polyelectrolyte and zinc oxide stacked structure as an interlayer in highly efficient and stable organic photovoltaic cells, J. Mater. Chem. A 1 (2013) 6446–6451.